WSRC-MS-2004-00286, Rev. 0
Distribution Category: Unlimited

Keywords: DWPF, pour spout pluggage, liquidus, crystallization, pouring

Retention: Permanent

HIGH LEVEL WASTE (HLW) PROCESSING EXPERIENCE WITH INCREASED WASTE LOADINGS (U)

Carol M. Jantzen, Alex D. Cozzi, and Ned E. Bibler
Savannah River Technology Center
Aiken, SC 29808

A paper for publication in the Symposium on Waste Management Technologies in Ceramic and Nuclear Industries, American Ceramic Society, Westerville, OH

HIGH LEVEL WASTE PROCESSING EXPERIENCE WITH INCREASED WASTE LOADINGS

Carol M. Jantzen, Alex D. Cozzi, and Ned E. Bibler
Savannah River Technology Center
Aiken, South Carolina 29808

ABSTRACT

The Defense Waste Processing Facility (DWPF) Engineering requested characterization of glass samples that were taken after the second melter (Melter #2) had been operational for ~5 months. After the new melter had been installed, the waste loading[‡] had been increased to ~38 wt% after a new quasicrystalline liquidus model had been implemented. The DWPF had also switched from processing with refractory Frit 200 to a more fluid Frit 320. The samples were taken after DWPF observed very rapid buildup of deposits in the upper pour spout bore and on the pour spout insert while processing the high waste loading feedstock. These samples were evaluated using various analytical techniques to determine the cause of the crystallization. The pour stream sample was homogenous, amorphous, and representative of the feed batch from which it was derived. Chemical analysis of the pour stream sample indicated that a waste loading of 38.5 wt% had been achieved. The data analysis indicated that surface crystallization, induced by temperature and oxygen fugacity gradients in the pour spout, caused surface crystallization to occur in the spout and on the insert at the higher waste loadings even though there was no crystallization in the pour stream.

INTRODUCTION

Characterization of three glass samples that were taken from the first DWPF replacement melter (Melter #2) were performed. The samples were taken after the second melter had been in operation for ~5 months, after the waste loading had been increased to ~38 wt%, e.g. after the new quasichemical liquidus model [1] had been implemented, and after DWPF switched from processing with Frit 200 (high in SiO_2) to a more fluid Frit 320. The DWPF had observed a very rapid buildup of deposits in the upper spout bore and on the pour spout insert while processing the high waste loading feedstock. Rapid deposition in these locations had not occurred prior to processing the high waste loaded feeds and stopped after waste loading was decreased.

The sample analyses performed included chemical composition (including noble metals), crystal content, and REDuction/OXidation (REDOX) expressed as the $Fe^{+2}/\Sigma Fe$ ratio. The three glasses consisted of the following:

- a pour stream sample taken while filling canister S01859 during processing of Sludge Batch 2 (SB2),
- a sample that was scraped from the 2 inch upper pour spout bore (Figure 1) using a 1-7/8" diameter rotating drill bit while the melter was hot; the material had grown/accumulated at or just below the transition from the riser to the pour spout,
- a sample of glass adhering to a Melter #2 Type I insert (Figure 1) that had spalled from the interior of the insert after it had cooled.

[‡] The waste loading (w) is defined thoughout this paper on a consistent basis, e.g. $w=100*[1-(g_{Li}/f_{Li})]$ where g_{Li} = grams of Li in 100 grams of glass and f_{Li} = grams of Li in 100 grams of frit

The samples were taken on August 28, 2003. The glass being processed at that time corresponded to DWPF batch 245.

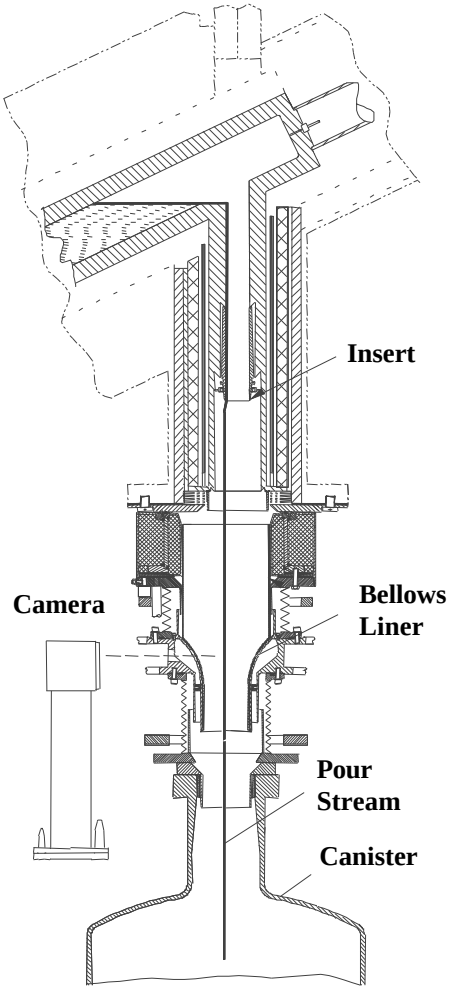

Figure 1. DWPF pour spout schematic showing location of the upper bore (section above the insert), the insert, the pour stream, and the canister.

BACKGROUND

The Savannah River Site has operated various pilot scale melters in support of the design of DWPF (Table I) since 1978. All have had prototypic risers and pour spouts. Two of the pilot scale melters experienced crystalline buildups in the pour spout risers and nozzles, and these case studies were examined for relevance to the current deposition problems.

The Project 1941 melter was ~½ the DWPF melt pool surface area and was initially dry fed a calcine oxide sludge and later slurry fed. The melter produced 74 tons of simulated waste glass. During the dry calcine feeding, a crystalline layer of ~9 inches thick formed at the bottom of the melter [2]. This material formed primarily during a 58 day idle at 1050°C. Upon probing the melter after the idle period, the deposits on the bottom of the melter floor were determined to be very dense (“hard”) and comprised 4 inches of spinel deposits [2]. A less dense spinel layer comprised the remaining 5 inches of deposits. When the 1941 large scale melter was shut down,

it was dismantled to evaluate its service life [3]. Additional crystalline deposits up to approximately 1 inch thick were found to have formed on the walls of the melter and in the riser and nozzle. The crystalline deposits found in the riser and nozzle of the 1941 melter were found to have almost completely plugged the riser [3]. When enough crystalline material had accumulated to fill the bottom of the 1941 melter, the deposits began to come out of the melter with the waste glass [3].

Table I. Pilot Scale Melters Operated In Support of DWPF Design.

Melter Designation	Melt Pool Surface Area (ft^2)*	Years of Operation	Pour Spout/Riser Pluggages	Crystal Buildup on Floor of Melter During Operation
Large Scale Project 1941 Melter	12	1978-1979	Yes	9”
Small Cylindrical Melter (SCM)	1.3	1979-1982	No	Several inches per campaign
Large Slurry Fed Melter (LSFM)	12	1982-1985	No	1/16-1/2”
Scale Glass Melter (SGM)	12.6	1986-1988	Yes	None
Integrated DWPF Melter System (IDMS)	3.14	1988-1994	No	None

* DWPF Design Basis of 228 lbs/hr or 8lbs/hr$(ft)^2$ times melt pool surface area (ft^2)

The large accumulations of three chemically distinct layers that eventually blocked the riser in the 1941 melter were attributed to the following:

- the bottom deposits were composed of Cr enriched spinels, an unidentified silicate, and a glass matrix enriched in alumina – this was attributed to corrosion of the K-3 refractory
- the second layer was composed of spinels, acmite, a glassy matrix, and entrapped waste glass of a normal (not alumina enriched) composition
- the top layer was similar to the second layer but did not contain entrapped waste glass.

Since the DWPF Melter #2 had not be idled at 1050°C nor had it been fed calcine feeds, this potential mechanism for pour spout crystallization was not considered relevant to the current accumulation of crystalline material.

The Scale Glass Melter (SGM) produced ~90 tons of glass in two years based on Frits 165, 168, and 200 and a reducing (formic acid) flowsheet. Crystalline deposits were not found in the SGM when the melter bottom was probed after the 5th melter Campaign (SGM-5) [4]. When the SGM was bottom drained after the 9th Campaign (SGM-9), no significant accumulations of deposits were observed [5]. However, in-situ formation of crystalline deposits did occur in the SGM melter pour spout and the deposition was similar to those experienced by DWPF Melter #2.

Deposition was experienced during the SGM-1 campaign due to a cool pour spout tip [6]. Temperatures were 980°C on the glass contact side near the glass disengagement point, 1040°C closer to the pour spout bore and600°C on the opposite side of the pour spout bore during steady state pouring [7]. Crystallization of these deposits resulted in frequent channel pluggages and reduced production rate ~50%.

Pluggages formed in the SGM-1 pour spout discharge tube on 10 different occasions. The pluggages were composed of visibly crystallized glass. Batch pouring aggravated plugging; pluggages appeared to become worse as the length of time between pours increased. Characterization of the size, composition, and volume fraction of the crystallized (devitrified) phases in the SGM-1 pour spout was used to interpret the thermal history of the glass [8]. The identification of acmite crystals indicated that the affected sections of the pour spout were as cool as ~700°C while the thermocouples indicated that this region was hotter. The large size of the crystals indicated that the crystals had formed in the pour spout at these low temperatures over long time periods.

The SGM-1 pour spout pluggage and associated interpretation of the thermal history [8] led to a redesign of the pour spout, e.g. better insulation and relocation of the thermocouples to accurately profile pour spout temperatures. After this redesign, the SGM did not experience severe pour spout pluggages even when processing waste loadings up to 42 wt%.[‡] This suggested that the temperature profiles in the DWPF Melter #2 pour spout were relevant to the current accumulation of crystalline material.

PILOT SCALE MELTER WASTE LOADINGS AND LIQUIDUS TEMPERATURES

The glass composition data from the SCM-2, the LSFM, and the SGM was compiled into a database [9]. Compositional data for the LSFM and SCM-2 was compiled from analyzed feed and frit compositions. Compositional data for the SGM campaigns was from analyzed glasses taken from full sized canisters. Compositional data for the Project 1941 melter could not be found. The analyzed glass composition data from the IDMS melter campaigns was available but the glass analyses from these melter campaigns was suspect for liquidus temperate predictions due to Cr_2O_3 contamination from the grinders used [10]. Since Cr_2O_3 content has a large impact on the liquidus temperature calculated from the quasicrystalline model [1], this data was not included in comparison of pilot scale melters and DWPF operational history, e.g. predicted liquidus and waste loading.

The data in reference 9 was used to calculate the DWPF liquidus temperature from the DWPF historic liquidus model [11], the DWPF liquidus temperature from the newly implemented quasicrystalline model [1], and the waste loading achieved based on the Li_2O content of the frit.[‡] A comparison of the predicted liquidus temperature model calculated two different ways is shown in Figure 2 while the comparison of the quasicrystalline liquidus temperature to waste loading is shown in Figure 3. The ordinary least squares equation of best fit for the data shown in Figure 2 is

$$\text{Quasicrystalline Liquidus (°C)} = -590.476 + 1.5276\ (\text{Historic Liquidus,°C}). \qquad (1)$$

with an adjusted R^2 of 0.82 and a Root Mean Square Error of 34.58. Figure 2 shows the following:

- there is a linear correlation between the historic and quasicrystalline liquidus models
- there is approximately a 36°C offset in the historic liquidus (1050°C) and the corresponding quasicrystalline liquidus (1013°C) at the DWPF liquidus temperature limit of 1050°C

[‡] The waste loading (w) is defined thoughout this paper on a consistent basis, e.g. $w=100*[1-(g_{Li}/f_{Li})]$ where g_{Li} = grams of Li in 100 grams of glass and f_{Li} = grams of Li in 100 grams of frit

- pilot scale melters such as the LSFM operated at lower liquidus values than the other pilot scale melters, e.g. SGM and SCM-2

A combination of the data displayed in Figure 2, the data given in reference 9, and the operating experiences summarized in Table I shows the following:

- the lower liquidus values experienced during the LSFM campaigns was associated with lower waste loadings in the range of 20-32 wt% when calculated from the frit Li_2O values
- the scale glass melter (SGM-6), which had a DWPF prototypic pour spout and ran reducing flow sheets, ran some very high waste loadings (up to 42 wt%) and no pour spout pluggages were experienced once the pour spout was insulated and the thermocouples relocated after the SGM-1 campaign.

EXPERIMENTAL

Elemental Analyses

The samples from Melter #2 were prepared for chemical analyses by pulverizing a portion of each in a Wig-L-Bug using agate balls and vial. The pulverized sample was sieved to <100-mesh (149 μm) and dissolved by two different dissolution methods to account for all the elements of interest.

A standard reference glass, Approved Reference Glass #1 (ARG-1), was analyzed at the same time as the unknowns. Each standard and each unknown was dissolved in quadruplicate and one replicate analysis of each sample was performed. The quadruplicate analyses were averaged to create the data in Table II. The dissolutions were analyzed by Inductively Coupled Plasma – Emission Spectroscopy (ICP-ES) and ICP Mass Spectroscopy (ICP-MS). The peroxide fusion analyses are reported in Table II preferentially because undissolved solids were found in some of the mixed acid digestions. Details are given elsewhere [9].

In order to provide a representation of the expected composition of the pour stream sample, the analysis of Slurry Mix Evaporator (SME) batch 245 and Melter Feed Tank (MFT) batch 245 were converted to oxides using the DWPF Product Composition Control System (PCCS). Table II gives the composition of the three DWPF samples as well as the composition of the SRTC Tank 40 qualification glass sample and the measured composition of SME Batch 245 and MFT batch 245.

The composition of the pour stream sample resembles the SRTC Tank 40 qualification glass made with Frit 320 in the Shielded Cells Facility in Al_2O_3, MgO, B_2O_3, CaO, CuO, Li_2O, MgO, MnO, P_2O_5, and U_3O_8 (Table II) as it should, i.e., the Tank 40 sample was representative. The pour stream sample resembles most of the major components as determined by analysis of SME batch 245 (Table II). This is verified in Table III as the ratios of most components in SME batch 245 divided by the concentrations in the pour stream sample (PC0033) are close to 1.0 as they should be. The SME batch 245 analyses appear to be biased high or the pour stream samples biased low for Al_2O_3, B_2O_3, CaO, Fe_2O_3, NiO and U_3O_8 by 15-20%. The MFT batch 245 analyses divided by the concentrations in the pour stream sample (PC0033) are ~1.0 except for the Al_2O_3 and B_2O_3 analyses which are biased by ~20% (Table II).

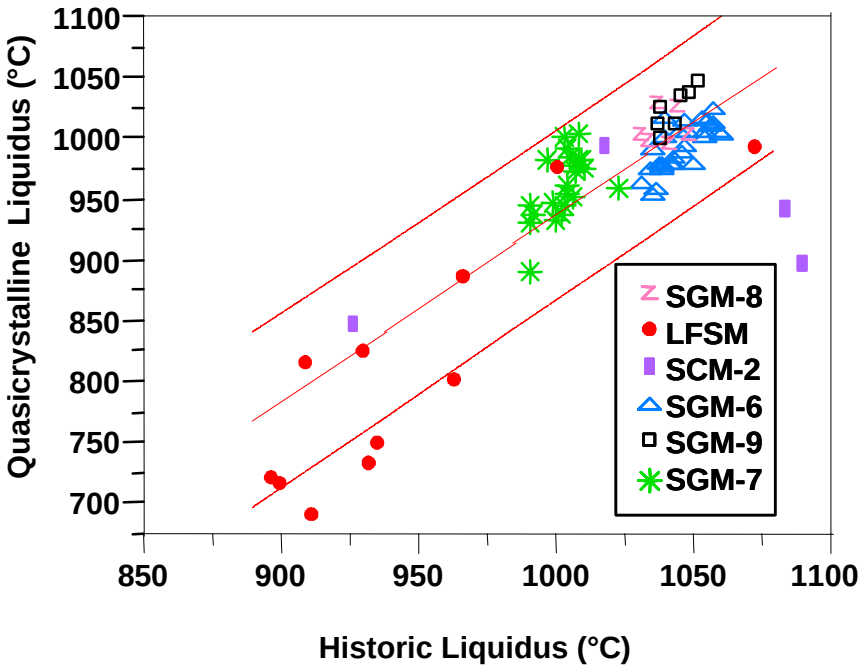

Figure 2. Comparison of the liquidus temperatures for various pilot scale melters calculated with the DWPF historic and quasichemical modes.

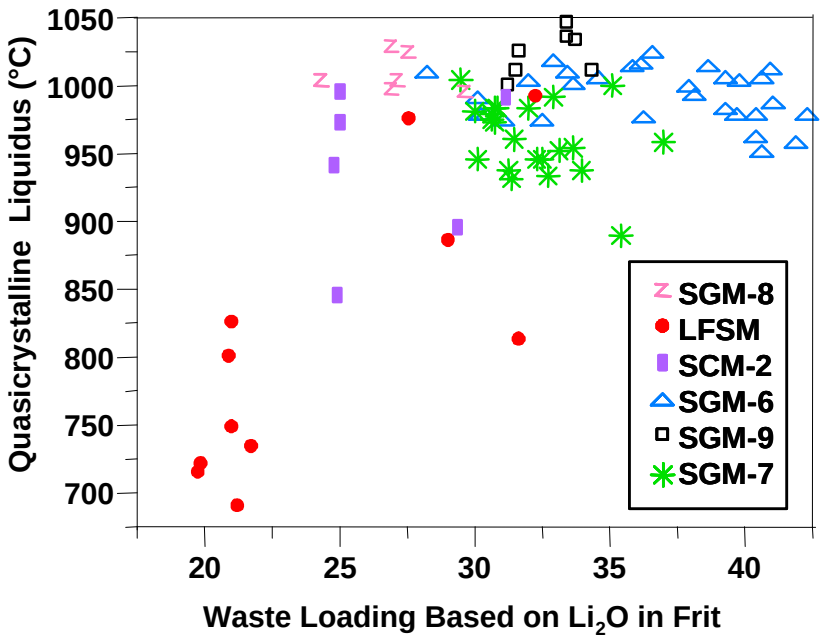

Figure 3. Comparison of the liquidus temperatures and waste loadings for various pilot scale melters calculated with the newly implemented DWPF quasicrystalline model.

The compositions of the analyses reported in Table II were used to calculate a predicted glass viscosity, liquidus temperature, and waste loading. The predicted viscosity based on the vitrified MFT product (43.48 poise) and the pour stream sample (46.05 poise) was in agreement to within 2.5 poise. The predicted liquidus based on the vitrified MFT 245 product (987°C) and the pour stream sample (997°C) was in agreement to within 10°C. The waste loadings predicted from the MFT (34.74 wt%) and the pour spout analyses (38.53 wt%) agree to within 3.79 wt%.

The composition of the upper pour spout bore sample (PC0006) was very different from the pour stream sample (PC0033) and very different from the MFT and SME analyses. The pour spout bore sample was deficient in Al_2O_3, B_2O_3, CaO, Li_2O, Na_2O, U_3O_8 and SiO_2 (Table III). Based on the relative Li_2O content of the pour stream sample (PC0033) relative to the bore sample (PC0006) it is estimated that the upper pour spout bore sample was ~62 wt% glass (Table IV). Based on the relative SiO_2 content of these samples it is estimated that the upper pour spout bore sample is ~52 wt% glass (Table IV). Compared to the pour stream, the upper pour spout bore sample was enriched in Cr_2O_3 over the pour stream sample by 35.9X, enriched in Fe_2O_3 by only 2.6X, and enriched in NiO by 15.4X. Based on the analyzed compositions given in Table II and the X-ray diffraction spectra, the number of moles of NiO, Cr_2O_3, and Fe_2O_3 over those reported in the pour stream were calculated. Based on these molar compositions it could be determined that 0.11 moles of $NiFe_2O_4$ and 0.034 moles of $NiCr_2O_4$ spinels comprised the remainder of the bore samples. When converted to weight percent, a mass balance indicated that the deposits were ~62 wt% glass, 25.78 wt% $NiFe_2O_4$ (trevorite) and 7.7 wt% $NiCr_2O_4$ (Table IV). The upper pour spout bore is also highly enriched in noble metal components; especially Rh_2O_3 and RuO_2 (Table V).

The insert sample (PC0031) was enriched the most in Cr_2O_3 over both the pour stream sample (PC0033) and upper pour spout bore sample (PC0006). The insert sample contains less Fe_2O_3 and NiO than the upper pour spout bore. This indicates that less $NiFe_2O_4$ spinels are accumulating in this area, e.g. the mass balance analyses indicate ~16.4 wt% $NiFe_2O_4$ (see Table IV). However, the high Cr_2O_3 content supported by the XRD identification of a Cr_2O_3 only phase. indicates that there may be a reaction occurring with the hot glass and the Cr in the Inconel® 690 alloy insert. That is, an oxidized film of Cr_2O_3 may be forming to which some molten glass adheres. Since the sample received had “spalled off” the insert as it cooled, it is likely that the sample contained a good deal of the oxidized Cr_2O_3 film from the Inconel® 690. The mass balance indicates that ~21 wt% Cr_2O_3 comprises the analyzed deposits. Table III presents the ratios of the pour stream sample major components to the other compositions from Table II. The insert sample is also enriched in noble metals (Table V).

Noble Metal Analyses

The solutions that resulted from the peroxide fusion of the three samples were analyzed by ICP-MS for noble metals. Concentrations in weight percent along with the respective concentrations measured in the SRTC Tank 40 qualification sample are given in Table V. The data from the SB2 pour stream and insert are also given in Table V for comparison. The peroxide fusion (PF) was used to ensure that all the refractory spinels in the pour spout and insert samples were dissolved because the noble metal, Ru as RuO_2, is most often in the center of an insoluble spinel crystal where it has acted as a nucleating site. Based on the PF data in Table V, the noble metals, Ru and Rh were 56 to 81 times more concentrated in the upper pour spout bore than in the pour stream. The Ru and Rh were 10 and >17 times more concentrated in the insert glass.

Table II. Measured Compositions of the DWPF Melter #2 Samples Compared to SRTC Tank 40 Glass and DWPF SME Batch 245 and MFT Batch 245 (in Oxide Wt.%)

Oxide	Dissolution/ Analysis Methods	Pour Stream (PC0033)	Upper Pour Spout Bore (PC0006)	Insert (PC0031)	SRTC TK 40 Glass[12]	SME Batch 245	MFT Batch 245
Ag_2O	PF/ICPMS	0.0072	BDL	0.006	NM	NM	NM
Al_2O_3	PF/ICPES	4.33	2.40	2.54	4.93	5.59	5.04
B_2O_3	PF/ICPES	4.33	<2.93	<2.68	4.87	5.21	5.26
BaO	PF/ICPES	0.03	0.02	0.01	NM	NM	NM
CaO	PF/ICPES	1.48	0.95	0.87	1.53	1.69	1.26
CdO	PF/ICPES	0.05	0.05	0.05	NM	NM	NM
Cr_2O_3	PF/ICPES	0.15	5.38	21.22	0.31[a]	0.12	0.11
CuO	PF/ICPES	0.09	0.07	0.03	0.14	0.03	0.03
Fe_2O_3	PF/ICPES	13.64	36.03	25.19	16.16	15.69	14.07
K_2O	PF/ICPES	BDL	BDL	BDL	NM	0.1381	0.10
La_2O_3	PF/ICPES	0.04	0.04	0.05	NM	NM	NM
Li_2O	PF/ICPES	4.75	2.93	3.48	5.30	4.85	5.16
MgO	PF/ICPES	1.28	1.22	1.48	1.30	1.31	1.10
MnO	PF/ICPES	1.67	2.35	3.29	1.84	1.73	1.54
Na_2O	MA/ICPES	11.01	6.30	6.26	12.61	11.39	11.02
NiO	PF/ICPES	0.60	9.25	5.84	0.74	0.71	0.63
P_2O_5	PF/ICPES	0.60	<0.63	<0.63	0.74	<0.22	NM
SiO_2	PF/ICPES	46.87	24.26	24.55	51.2	45.67	48.11
SnO_2	PF/ICPES	0.21	0.20	0.19	NM	NM	NM
SrO	PF/ICPES	0.30	0.20	0.20	NM	NM	NM
Rh_2O_3	PF/ICPMS	0.0033	0.271	0.058	NM	NM	NM
RuO_2	PF/ICPMS	0.030	1.712	0.296	NM	NM	NM
TiO_2	PF/ICPES	0.04	0.03	0.11	NM	0.05	0.05
U_3O_8	PF/ICPES	3.45	2.63	2.45	4.06	4.22	3.80
ZnO	MA/ICPES	0.09	0.16	0.17	NM	NM	NM
ZrO_2	MA/ICPES	0.07	0.03	0.03	NM	BDL	0.09
SUM (w/o <)		95.12	96.48	98.37	105.73	98.4	97.37
Calculated Viscosity @1150°C (poise)		46.05	N/A	N/A	38.99	35.91	43.48
Calculated Liquidus (°C)		997	N/A	N/A	1056	1038	987
Calculated WL (Li_2O)		38.53[b]	N/A	N/A	36.10	39.32[b]	34.74[b]

(NM-Not Measured; BDL-Below Detection Limit; N/A-Not Applicable; MA-Mixed Acid dissolution; PF- Peroxide Fusion dissolution; WL-Waste Loading)

[a] Sample prepared in stainless steel grinder for Sludge Batch 2 (SB-2) qualification with Frit 320.

[b] Calculated using a value for Li_2O in the normalized frit of 8.13 wt% based on a weighted average of Frit 320 Lots 5, 8, and 13 in the ratio of 1:1:2.

Table III. Ratio of Major Components of the Pour Stream Sample to the Upper Pour Stream Bore Sample, to the Insert Sample, and to the SME and MFT 245 Analyses

	Insert /Pour Stream	Upper Pour Spout Bore /Pour Stream	SME batch 245/ Pour Stream	MFT batch 245/ Pour Stream
Al_2O_3	0.59	0.55	1.29	1.16
B_2O_3	N/A	N/A	1.20	1.21
CaO	0.59	0.64	1.14	0.85
Cr_2O_3	141.47	35.87	0.8	0.73
Fe_2O_3	1.85	2.64	1.15	1.03
Li_2O	0.73	0.62	1.02	1.09
MgO	1.16	0.95	1.02	0.86
MnO	1.97	1.41	1.04	0.92
Na_2O	0.56	0.57	1.03	1.01
NiO	9.73	15.42	1.18	1.05
SiO_2	0.52	0.52	0.97	1.03
U_3O_8	0.71	0.76	1.22	1.10

Table IV. Mass Balance for Samples Based on Data in Table II.

Calculated (Wt%)	Pour Stream (PC0033) Frit 320	Upper Pour Spout Bore (PC0006) Frit 320	Insert (PC0031) Frit 320
Glass (Based on Li_2O in Pour Stream	100	62	73
$NiFe_2O_4$ Spinel	0	25.78	16.4
$NiCr_2O_4$ Spinel	0	7.70	0
Cr_2O_3	0	0	21.07
$RuO_2 + Rh_2O_3$	0.03	1.98	0.36
SUM	100.03	97.46	110.83

Table V. Comparison of the Noble Metals (wt.%) of the SRTC Tank 40, Pour Stream, Upper Pour Spout Bore, and Insert Glasses.

Isotope	SB2 Pour Stream Glass (August 2002)	SB2 Insert Glass (August 2002)	SB2 Pour Stream Glass (PC0033)	SB2 Upper Pour Spout Bore (PC0006)	SB2 Insert (PC0031)	Ratio Insert/ Pour Stream[b]	Ratio Upper Spout Bore/ Pour Stream
Ru	NA	NA	0.023	1.3	0.23	10	56.52
Rh	NA	NA	0.0027	0.22	0.047	17.41	81.48

[b] This ratio should be ~0.47 because of dilution of the glass components by material from the insert (see text).

REDOX Analyses

Portions of the pour stream sample (PC0033) were pulverized using a non-metallic Wig-L-Bug in the SRTC Shielded Cells. The Environmental Assessment (EA) glass, a REDOX standard, was prepared by grinding it in a Tekmar grinder outside the SRTC Shielded Cells. The EA glass standard has a REDOX, expressed as (Fe^{2+}/• Fe), of ~ 0.18 [13]. Dissolutions of triplicate samples were performed using <100 mesh material prepared in the same manner as the material for compositional analysis. The dissolution was performed in the SRTC Shielded Cells. The spectrophotometric analysis were performed in a radiohood.

Table VI gives the results of the triplicate REDOX analyses of the pour stream glass and the EA glass standard. The measured REDOX of the EA glass was greater than expected.

Microscopic investigation of the EA glass standard indicated that it was contaminated with metal filings from the Tekmar grinder. This did not affect the REDOX of the pour stream sample since it was ground with a non-metallic Wig-L-Bug.

A second pour stream sample and EA glass standard were both ground with the Wig-L-Bug to prevent metal contamination and the REDOX was re-measured in triplicate in the SRTC Shielded Cells (see Table VI). This set of analyses gave a blank corrected EA glass standard value of $Fe^{+2}/\bullet$ Fe=0.24 versus the reported standard value of 0.18 indicating that the problems with iron contamination had been avoided by using the Wig-L-Bug. The average remeasured values for the triplicate (PC0033) samples were 0.20 in agreement with the previous values determined in Table VI. The predicted REDOX of SME batch 245 was 0.17 based on the {[F]-[3N]} REDOX correlation [14] and 0.15 based on the new Electron Equivalents REDOX correlation [15]. This indicates that the REDOX model [1,15] predictions and batching in the DWPF SRAT and melter are working correctly and are on target.

Table VI. REDOX of Pour Stream Glass Prepared in the SRTC Shielded Cells.

Set	Sample	$Fe^{+2}/\bullet$ Fe Standard Value	Target $Fe^{+2}/\bullet$ Fe of Pour Stream	Blank Corrected Average ($Fe^{+2}/\bullet$ Fe)
1	EA Standard	0.18	N/A	0.41*
1	Pour Stream	N/A	0.15-0.17	0.20
2	EA Standard	0.18	N/A	0.24
2	Pour Stream	N/A	0.15-0.17	0.20

* iron or steel contamination observed

Contained Scanning Electron Microscopy (CSEM)

The <200 mesh crushed samples from the chemical analyses were used for Contained Scanning Electron Microscopy with Energy Dispersive Spectroscopy (CSEM/EDS). The CSEM analysis of the pour stream sample revealed uniformity across the entire sample and showed no crystallization. The EDS spectrums of various pour stream samples also indicated homogeneous DWPF-type glass.

The insert sample viewed at 500x appeared to have more surface texture than a typical glass sample. A single grain was examined that had a coating of a Fe and Cr rich material compared to the right hand side of the same grain that had an EDS spectra typical of glass. The coating appeared to be a portion of the Inconel® 690 to which the once molten glass had adhered.

The CSEM/EDS of the insert sample revealed copious amounts of spinels. Some of the spinels were more enriched in Cr than others. The non-crystalline portion of the sample gave a spectra typical of glass and demonstrated that the U component is in the glassy phase and does not participate in the crystallization. The EDS spectra did not indicate that the spinels were associated with RuO_2.

Contained X-ray Diffraction Analysis (CXRD)

Three different portions of the pour stream were analyzed by CXRD. The XRD pattern of the pour stream samples was typical of a borosilicate glass and free of any indicators of crystalline matter except for potential stainless steel (ss) contamination from grinding.

The CXRD analysis of the insert sample indicated the presence of glass, spinel, and chrome oxide (eskolaite). The spinel phase most likely resembles trevorite with chromium partially substituting for iron and iron partially substituting for nickel, based on the CSEM analyses.

The CXRD analysis of the upper pour spout bore sample indicated the presence of glass, spinel, and RuO_2. This is consistent with the chemical analyses of the upper pour spout bore sample being enriched in RuO_2 compared to the pour stream glass (See Table II and Table V). Likewise, there is an 81% enrichment of Rh_2O_3 (Table V). Therefore some mechanism is causing the RuO_2 and Rh_2O_3 to accumulate in the upper pour spout bore area over and above the amount of accumulation of the spinel forming components.

The spinel identified in the upper pour spout bore sample (PC0006) is a mixture of ~26 wt% trevorite ($NiFe_2O_4$) and ~8 wt% $NiCr_2O_4$ (see Table IV). The Cr_2O_3 is enriched in these deposits ~36X (Table III) relative to the amount in the pour stream sample (PC0033). Corrosion (oxidation) of the Inconel® 690 lining of the bore in this oxidizing environment on the pour spout is the most likely the primary source of the Cr^{+3}. Therefore, the molten glass and the Inconel® 690 pour spout lining are chemically interacting in this hot oxidizing environment. That is to say that the oxygen fugacity in the upper pour spout bore is more reducing than that of the insert (air $\log f_{O_2} = -0.68$) but considerably more reducing than that of the melt pool (melt pool $\log f_{O_2} = -5.5$). Therefore, the region of the upper pour spout bore experiences large gradients in both temperature and oxygen fugacity which can induce spinel crystallization, e.g. the measured activation energy for spinel crystallization in DWPF type waste glass in an oxidizing atmosphere ($Fe^{+2}/\bullet$ Fe~0 at a $\log f_{O_2} = -0.68$) is 17.7 kcal/mole while the activation energy for spinel crystallization from a reducing glass ($Fe^{+2}/\bullet$ Fe~0.5 at a $\log f_{O_2} = -7$) is only 2.9 kcal/mole [16]. Therefore, crystallization of spinel is more rapid in the oxidizing atmosphere of the upper pour spout bore and insert than in the melt pool.

DISCUSSION

Volume Versus Surface Crystallization

Volume crystallization[§] can involve rapid nucleation of the melt pool. Once formed, the type of $NiFe_2O_4$ spinel crystals that occur in DWPF waste glass melts are refractory (reported melt temperature of 1660±10ºC [17]) and cannot be redissolved into the melt pool at the DWPF operating temperature of 1150ºC. Therefore, the DWPF liquidus temperature model focused on preventing heterogeneous volume crystallization rather than preventing surface crystallization [18].

Surface crystallization[**] has not been considered to be problematic in nuclear waste glass melters since spinel precursors ($NaFe_2O_4$ [19,20] and $LiFe_2O_4$ [21]), which can redissolve in the melt pool, have been found to form at the melt-atmosphere interface rather than insoluble $NiFe_2O_4$ spinels. Moreover, waste glass melts have been found to form a protective layer along the refractory walls which minimizes spinel formation in the melt pool from the refractory surfaces [22, 3], as long as the melt pool agitation or bubbling does not directly impinge on the

§ crystal growth begins from either homogeneous or heterogeneous nucleation sites with a melt [27]; volume crystallization of the spinel primary liquidus phase has been shown to be heterogeneous forming on melt insolubles in the waste such as RuO_2 [11,13].

** crystal growth begins (i.e. nucleates) from the melt-atmosphere interface or the melt-container (melt-refractory) interface and grows perpendicular to the interface

melter walls. Surface crystallization can, however, be problematic where metallic materials of construction contact glass at temperatures lower than the liquidus temperature.

Pour Stream Sample: Volume Crystallization

Visual observation of the pour stream sample (PC0033) showed the sample to be typical of a DWPF-type glass (opaque and reflective). Compositional analysis by ICP-ES demonstrated a correlation between the pour stream sample and the MFT batch 245. The MFT analysis predicted a glass viscosity within 2.5 poise of the pour stream sample calculated viscosity. The MFT 245 analysis predicted a liquidus within 10ºC of the pour stream calculated liquidus. The SME and pour stream calculations for waste loading agree to within 0.35 wt%, while the MFT and the pour stream calculations for waste loading agree to within 3.79 wt%. The measured REDOX was $Fe^{+2}/\Sigma Fe = 0.2$ while the SME 245 target based on the {[F]-[3N]} correlation was 0.17 and the target based on the Electron Equivalents model was 0.15. Therefore, the viscosity [11], liquidus [1], and REDOX [14,15] models based on feed analyses appear to be adequately controlling the DWPF glass properties.

The pour stream sample, analyzed by CXRD in triplicate, contained no crystals and was totally amorphous. Therefore, there is no crystallization of spinel in the melt pool, which means that the liquidus model [1] is predicting and preventing volume crystallization in the melt pool as it was intended to do.

Pour Spout and Bore Samples: Surface Crystallization

Noble Metals: The pour spout insert sample was enriched in Ru 10X and Rh 17X over that present in the pour stream. The Ru as RuO_2 and the Rh as Rh_2O_3 could be acting as nuclei for the crystallization of the 16.4 wt% $NiFe_2O_4$ spinel, but during CSEM no RuO_2 or Rh_2O_3 were observed to be associated with or acting as nuclei for the crystallization of $NiFe_2O_4$ spinel. The role of the RuO_2 and Rh_2O_3 is indeterminate although an intermediate oxide compound $RhCrO_3$, is known to occur [23]. In addition, if RuO_2 is reduced to Ru° locally in contact with the Inconel® 690 alloy, there are known solid solutions between Ru° and Ni° [24].

The upper pour spout bore contained 1.71 wt% RuO_2 and 0.27 wt% Rh_2O_3 in the deposits analyzed which is a 56X and 81X increase of these components in the pour spout bore samples compared to the pour stream. The CXRD analysis confirms the presence of an amorphous phase, a spinel phase, and RuO_2. In this case spinel and RuO_2 deposition could be synergestic.

Crystalline Deposits: Spinel and Cr_2O_3: The DWPF liquidus model was developed to prevent volume crystallization of the melt pool at the normal melter operational temperatures, e.g. between 1050-1150°C, at normal oxygen fugacities experienced in waste glass melters, e.g. between $\log f_{O_2} = -2$ and $\log f_{O_2} = -9$. Operation of the SGM melter, specifically SGM Campaign 6, at waste loadings in excess of 38 wt% (Figure 3), e.g. in the range in which DWPF experienced severe pour spout crystallization, is achievable if the pour spout is well insulated and kept hot.

As the glass flows up the riser, down the pour spout, and over the pour spout insert the following occurs:

- cooler temperatures are encountered, i.e., <1050°C which is below the liquidus of the glass being poured which enhances the kinetics of crystallization of spinel

- more oxidizing atmospheres (fugacities) are encountered, e.g. air $\log f_{O_2} = -0.68$ which enhances the kinetics of the crystallization of spinel [16] relative to the reducing atmosphere of the melt pool
- cooler Inconel® 690 surfaces are contacted that act as heat sinks inducing surface crystallization instead of bulk or volume crystallization
- cooler Inconel® 690 surfaces are contacted that are themselves being oxidized due to exposure to air and these surfaces release Cr_2O_3, which can further serve to nucleate spinels

Such crystallization in the melter riser, specifically in the tip of the pour spout channel had been observed during the first campaign of the DWPF pilot SGM. Crystallized deposits formed on ten separate occasions and were attributed to the fact that the tip of the pour spout channel lacked sufficient insulation which caused this region to be significantly cooler, ~800°C, than the thermocouples were indicating. Additional insulation and relocation of the thermocouples remediated the pluggage difficulties.

If the DWPF pour spout insert and upper pour spout bore are cooler than the liquidus temperature predicted by the DWPF Product Composition Control System (PCCS), e.g. a liquidus temperature of 987°C predicted for MFT 245 (Table II) and a liquidus of 997°C predicted from the pour stream analysis (Table II), then surface nucleation of crystals on these cooler surfaces is more likely to occur. This is because a higher waste loaded melt is closer to its crystallization temperature when it exits the melter than a lower waste loaded melt. Thus, unless a higher waste loaded melt is moved through the cooler region very rapidly, the glass crystallizes instead of "undercooling" to an amorphous state. In other words, the riser temperature profile is too steep (the bore is not hot enough) which allows spinels to form at higher waste loadings because the cooling rate is not fast enough in this region.

Heat Sink Induced Crystallization: In order to demonstrate the importance of cooling rate, dT/dt (where T is temperature in °C and t is time in seconds) calculations were performed assuming different temperatures for the upper pour spout bore ranging from 1100°C (the temperature of the LSFM bore), to 1040°C (the temperature of the SGM-1 bore), to 980°C (the temperature of the SGM-1 pour tip). The equation for the lowering of temperature with time for a finite body in contact with a heat sink (substrate) at a lower temperature may be written as follows [25]

$$\frac{T_t - T_s}{T_{t=0} - T_s} = \exp(t\left(\frac{K_m}{\rho \bullet C_p}\right)d^2) \qquad (2)$$

T_t = temperature at time t (°C)
T_s = temperature of the substrate (°C)
K_m = thermal conductivity at the melting point (cal/cm sec °C)
C_p = specific heat (cal/g °C)
d = thickness (or radius if the cooling body is spherical) in cm
ρ = density in g/cm^3 at the melt temperature

Since DWPF glasses undergo Newtonian cooling, the term hd can be substituted for K_m where h is the heat transfer coefficient. Taking the logarithms of Equation 2 and differentiating

with respect to t, the following expression for an instantaneous cooling rate (Q) can be calculated:

$$Q \equiv \frac{dT}{dt} = (T_t - T_s)\left(\frac{h}{\mathrm{r} \bullet C_p}\right)d \qquad (3)$$

where h = heat transfer coefficient (cal/cm^2 sec °C)

Note that the latent heat of fusion (ΔH_f) does not enter the calculation since crystallization only intervenes when the cooling rate is not great enough to prevent diffusional ordering from occurring [25]. The following parameters were used to approximate h, ρ, d, T_t, T_s, and C_p for DWPF type glass for a relative comparison of how substrate temperature can impact surface crystallization:

- radius of the DWPF pour stream ~0.25 cm
- $T_t = T_L$ (°C)
- T_s = varied from 900°C to 1150°C
- ρ = 2.47 g/m^3 for a high-Fe 131 glass [26,27] which is similar to the measured room temperature density in this report of 2.503 g/cm^3
- C_p = specific heat at T_s for a high-Fe 165 glass [28] which is similar to a high-Fe Frit 320 glass
- h = 1.7 cal/cm^{2}sec°C valid for SRL 131/Stage 1 waste glass above 900°C.

This allows Q ≡ dT/dt, a critical cooling rate to avoid crystallization to be estimated for DWPF glasses depending on the temperature of the Inconel® 690 substrate. This calculation is only approximate but serves to illustrate how much more rapidly the glass must be cooled as the Inconel® 690 substrate temperatures decrease, i.e., as the • T• T_L-T_s, the degree of undercooling increases. For example, at the liquidus temperature of 997°C for the DWPF pour spout sample (PC0003) analyzed in this report (see Table II) and a heat sink (pour spout) temperature of 980°C (the temperature of the pour spout tip near the disengagement point for SGM-1 from reference 7), a cooling rate of ~+9.7°C/sec is needed to prevent crystallization (see Table VII). At the pour spout bore temperature of SGM-1, e.g. 1040°C [7], a cooling rate of <1°C/sec is needed to prevent crystallization. If the pour spout were hotter, e.g. 1100°C, then a slower cooling rate is needed to prevent crystallization. This latter substrate temperature is consistent with the riser and pour spout temperatures reported during the 5th campaign of the LSFM melter, e.g. in the range of 1125°C ± 10°C and 1075°C ± 10°C, respectively, when no pour spout pluggages were observed [29].

For a melt with a liquidus of 1050°C, the cooling rates necessary to prevent crystallization at 980°C, 1040°C, and 1100°C become higher, e.g. 38°C/sec, +6°C/sec and <1°C/sec, respectively. So, more rapid cooling rates are necessary for the same substrate temperatures at higher waste loadings when the liquidus temperatures are higher. This can also be stated as more rapid cooling rates are necessary for larger undercoolings (• T), e.g. larger differences between T_L and T_s. It should also be noted that the larger the undercooling the more rapid the nucleation rate in glasses [30].

This suggests that if the DWPF pour spout bore or insert region is not sufficiently hot enough that the higher waste loaded glasses may be cooling off too slowly which allows surface nucleation of spinels on the inside of the upper bore. This, in conjunction with the more rapid nucleation of spinels in oxidizing environments and the availability of excess Cr_2O_3 from Inconel® 690 oxidation, has led to increased deposition in the spout and insert. This is consistent with the operating history of the LSFM which had a pour spout temperature of ~1075°C, poured lower waste loaded glasses, and did not have any pour spout pluggages. It is also consistent with the hotter spout designed for SGM after the 10 pour spout pluggages experienced when the pour spout tip was 980°C. Once the SGM was redesigned, it was able to pour glasses with calculated waste loadings up to ~42 wt% (see Figure 3). It should also be noted that the current DWPF melts have calculated viscosities in the range of the glasses melted during SGM campaign 6 during the pouring of canister six (SGM 6-6).

Table VII.Variation of Critical Cooling Rate with Heat Sink and Liquidus Temperatures.

Heat Sink Temperature (°C)	Melter Reference	Instantaneous Cooling Rate Needed for Glass with Liquidus of 997°C (°C/sec)	Instantaneous Cooling Rate Needed for Glass with Liquidus of 1050°C (°C/sec)
980	SGM-1 Tip of Pour Spout Before Insulation	9.7	38
1040	SGM-1 Bore Before Insulation	<1	6
~1100	LSFM Average in riser and bore	<<1	<1

Inconel® 690 Oxidation and Induced Crystallization: Oxidation of Inconel® 690 to Cr_2O_3 rich oxide is evidenced by the mass balance of the pour spout insert samples analyzed in this report, e.g. the sample was ~73 wt% glass, 16.4 wt% $NiFe_2O_4$, and 21 wt% Cr_2O_3. At the temperature of the pour spout insert, and indeed anywhere between 800-1100°C, Inconel® 690 can rapidly oxidize to form a protective chrome oxide layer [31,32] even in the presence of Fe_2O_3 and FeO [33]. DWPF melts having an $Fe^{+2}/\Sigma Fe$ ratio=0.2 have a corresponding oxygen fugacity ($\log f_{O_2}$) of -5.5. At this oxygen fugacity and any oxygen fugacity more positive than $\log f_{O_2}$ =-10, Ni-rich alloys such as Inconel® 690 decompose to $NiCr_2O_4$ and NiO [32]. This "free" NiO further complexes with the Fe_2O_3 in DWPF glass forming $NiFe_2O_4$ which depletes the Inconel® 690 in NiO leaving an enrichment in Cr_2O_3 deposits. This is evidenced by the relative positions of the Inconel® 690 alloy composition (Figure 4 point A) to the insert deposit composition (Figure 4 point C in mole percentage of Cr and Ni. Path AC in Figure 4 indicates that the insert deposits form by oxidation of Inconel® 690 and NiO depletion.

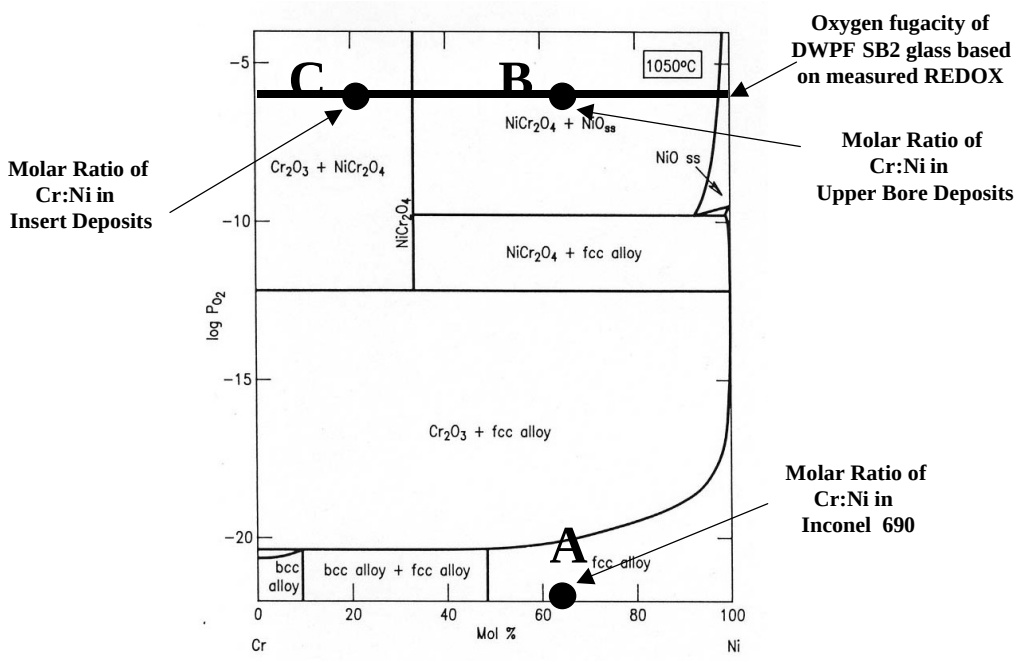

Figure 4. Binary phase diagram at 1050°C demonstrating the phases that are formed upon oxidation of a Ni-Cr alloy like Inconel® 690 [32].

The mass balance of the upper pour spout bore sample also indicated that the sample was Cr_2O_3 enriched, e.g. ~62 wt% glass, 25.8 wt% $NiFe_2O_4$, and 8 wt% $NiCr_2O_4$. Figure 4 readily shows that the Ni:Cr mole percentage of Inconel® 690 (point A) is the same as the ratio in the upper pour spout bore deposits (point B). The NiO released by Inconel® 690 oxidation further complexes with the Fe_2O_3 in DWPF glass forming $NiFe_2O_4$ as in the deposition of the insert deposits. These are the two main spinel components determined to be in the upper pour spout bore by mass balance (see Table III). This is evidenced by the relative positions of the Inconel® 690 alloy composition to the upper pour spout bore deposit composition to the insert deposit composition shown in Figure 4. These compositions represent the molar percentages of Cr and Ni in the deposits and in the alloy and indicate that the deposits form by oxidation of Inconel® 690 (path AB in Figure 4).

CONCLUSIONS

The Defense Waste Processing Facility (DWPF) Engineering requested characterization of three glass samples that were taken from Melter #2 after the waste loading had been increased and after rapid deposition had occurred in the DWPF pour spout region. The pour stream sample was determined to be homogenous, amorphous, and representative of feed tank chemistry from which it was derived. This indicated that the DWPF viscosity, liquidus, and REDOX models are keeping the DWPF process in control.

The most likely mechanism by which the severe crystallization of the pour spout and insert occurred are the temperature and oxygen fugacity (oxidation) gradients in the DWPF pour spout in conjunction with the higher waste loadings. The DWPF liquidus model was developed to prevent volume crystallization of the melt pool at the normal melt pool temperatures, e.g. between 1050-1150°C, and at the normal oxygen fugacities experienced in waste glass melters,

e.g. between $\log f_{O_2}$ = -2 ($Fe^{+2}/\Sigma Fe$=0.09) and $\log f_{O_2}$ = –9 ($Fe^{+2}/\Sigma Fe$=0.33). Operation of the SGM melter, specifically SGM Campaign 6, at waste loadings in excess of 38 wt% (Figure 3), i.e., in the range in which DWPF experienced severe pour spout crystallization, is achievable if the pour spout is well insulated and kept hot.

If the DWPF pour spout insert and upper pour spout bore are cooler than the liquidus temperature predicted by the DWPF PCCS, then surface nucleation of crystals on these cooler surfaces is more likely to occur. This is because a higher waste loaded melt is closer to its crystallization temperature when it exits the melter than a lower waste loaded melt. Thus, unless a higher waste loaded melt is moved through the cooler region very rapidly, the glass crystallizes instead of "undercooling" to an amorphous state. In other words, the riser temperature profile is too steep (the bore is not hot enough), which allows spinels to form at higher waste loadings because the cooling rate is not fast enough in this region.

Knowing that the DWPF pour spout bore and insert regions are more oxidizing than the melt pool and not sufficiently hot enough allows higher waste loaded glasses to cool too slowly. In other words, the degree of undercooling is too great, and the surface nucleation of spinels on the inside of the upper bore, spout, and insert can occur. The surface nucleation of spinels in the cooler more oxidizing regions of the pour spout is further enhanced in oxidizing environments because the activation energy of spinel nucleation is more rapid (17.7 kcal/mole) than in reducing environments (2.9 kcal/mole). In addition, the oxidative corrosion of Inconel® 690 provides excess Cr_2O_3 nuclei that can act as heterogeneous nuclei for spinel growth.

REFERENCES

[1] K.G. Brown, C.M. Jantzen and G. Ritzhaupt, **"Relating Liquidus Temperature to Composition for Defense Waste Processing Facility (DWPF) Process Control,"** WSRC-TR-2001-00520, Westinghouse Savannah River Co., Aiken, SC (October 2001).

[2] M.J. Plodinec, **"Long-Term Waste Management Progress Report Small-Scale Electric Meter, IV. Effects of Feed Mixing and Segregation on Glass Melting,"** U.S. DOE Report DPST-79-227, E.I. duPont deNemours & Co., Savannah River Lab., Aiken, SC (January 1979).

[3] W.N. Rankin, P.E. O'Rourke, P.D. Soper, M.B. Cosper, and B.C. Osgood, **"Evaluation of Corrosion and Deposition in the 1941 Melter,"** U.S. DOE Report DPST-82-231, E.I. duPont deNemours & Co., Savannah River Lab., Aiken, SC (March 1982).

[4] C.M. Jantzen, **"Lack of Slag Formation in the Scale Glass Melter,"** U.S. DOE Report DPST-87-373, E.I. duPont deNemours & Co., Savannah River Lab., Aiken, SC (April 1987).

[5] M.R. Baron and M.E. Smith, **"Summary of the Drain and Restart of the DWPF Scale Glass Melter, "** U.S. DOE Report DPST-88-481, E.I. duPont deNemours & Co., Savannah River Lab., Aiken, SC (May 1988).

[6] A.F. Weisman, **"Run Summaries from SGM-1, SGM-3, and SGM-4,"** U.S. DOE Report DPST-86-862, E.I. duPont deNemours & Co., Savannah River Lab., Aiken, SC (1986).

[7] A.F. Weisman, J.L. Mahoney, M. Rodman, K.R. Crow, D.M. Sabatino, and G.A. Griffin, **"Scale Melter Startup Review,"** U.S. DOE Report DPST-86-361, E.I. duPont deNemours & Co., Savannah River Laboratory, Aiken, SC (April 1986).

[8] C.M. Jantzen, **"Devitrification of Scale Melter Glass in Riser Heater,"** U.S. DOE Report DPST-86-461, E.I. duPont deNemours & Co., Savannah River Lab., Aiken, SC (May 1986).

[9] C.M. Jantzen, A.D. Cozzi, and N.E. Bibler, **"Characterization of Defense Waste Processing Facility (DWPF) Glass and Deposit Samples from Melter #2,"** U.S. DOE Report WSRC-TR-2003-00504, Rev. 0, Westinghouse Savannah River Co., Aiken, SC (April 2004).
[10]M.K. Andrews and J.R. Harbour, **"Chromium Levels in Feed and Glass for DWPF Startup Melter Campaigns,"** U.S. DOE Report WSRC-TR-95-0368, Westinghouse Savannah River Company, Aiken, SC (September 1995).
[11]C.M. Jantzen, **"Relationship of Glass Composition to Glass Viscosity, Resistivity, Liquidus Temperature, and Durability: First Principles Process-Product Models for Vitrification of Nuclear Waste,"** Proceed. 5th Intl. Symp. Ceram. in Nucl. Waste Mgt., G.G. Wicks, D.F. Bickford, and R. Bunnell (Eds.), Am. Ceram. Soc., Westerville, OH, 37-51 (1991).
[12]A.D. Cozzi, N.E. Bibler, T.L. Fellinger, J.M. Pareizs, and K.G. Brown, **"Vitrification of the DWPF SRAT Cycle of the Sludge-Only Flowsheet with Tank 40 Radioactive Sludge Using Frit 320 in the Shielded Cells Facility,"** U.S. DOE Report WSRC-RP-2002-00022, Rev. A, Westinghouse Savannah River Co., Aiken, SC (January 2002).
[13]C.M. Jantzen, N.E. Bibler, D.C. Beam, C.L. Crawford, and M.A. Pickett, **"Characterization of the Defense Waste Processing Facility (DWPF) Environmental Assessment (EA) Glass Standard Reference Material"**, WSRC-TR-92-346, Rev. 1, Westinghouse Savannah River Co., Aiken, SC (June 1994).
[14]K.G. Brown, C.M. Jantzen, and J.B. Pickett, **"The Effects of Formate and Nitrate on Reduction/Oxidation (Redox) Process Control for the Defense Waste Processing Facility (DWPF),"** WSRC-RP-97-34, Westinghouse Savannah River Co., Aiken, SC (February 1997).
[15]C.M. Jantzen, J.R. Zamecnik, D.C. Koopman, C.C. Herman, and J.B. Pickett, **"Electron Equivalents Model for Controlling REDuction/OXidation (REDOX) Equilibrium During High Level Waste (HLW) Vitrification,"** U.S. DOE Report WSRC-TR-2003-00126, Westinghouse Savannah River Co., Aiken, SC (May 9, 2003).
[16] C.M. Jantzen, D.F. Bickford, and D.G. Karraker, **"Time-Temperature-Transformation Kinetics in SRL Waste Glass,"** Adv. in Ceramics, 8, Am. Ceram. Soc., Westerville, OH, 30-38 (1984).
[17]A.E. VanArkel, E.J.W. Verwey, and M.G. VanBruggen, **"Ferrites I,"** Rec. Trav. Chim. 55, 331-339 (1936).
[18]C.M. Jantzen and K.G. Brown, **"Quasicrystalline Approach to Liquidus Temperature Prediction in Nuclear Waste Glasses,"** in preparation for J. Non-Crystalline Solids.
[19]M.J. Plodinec, **"Long-Term Waste Management Progress Report Small–Scale Electric Melter: II. Slag Formation,"** U.S. DOE Report DPST-78-453, E.I. duPont deNemours & Co., Savannah River Laboratory, Aiken, SC (August 1978).
[20]I.E. Grey and C. Li, **"New Silica-Containing Ferrite Phases in the System $NaFeO_2$-SiO_2,"** J. Solid State Chemistry, 69 [1], 116-125 (1987).
[21]J.D. Vienna, personal communication, Pacific Northwest National Laboratory (2002).
[22]C.M. Jantzen, K.G. Brown, K.J. Imrich, and J.B. Pickett, **"High Cr_2O_3 Refractory Corrosion in Oxidizing Melter Feeds: Relevance to Nuclear and Hazardous Waste Vitrification,"** Env. Issues and Waste Management Technologies in the Ceramic and Nuclear Industries, Vol. IV Ceram. Trans., V. 93, J.C. Marra and G.T. Chandler (Eds.), Am. Ceram. Soc., Westerville, OH, 203-212 (1999).
[23]I.S. Shaplygin, I.I. Prosychev, and V.B. Lazarev, Zh. Neorg. Khim 26 [11] 3081-3083 (1981).
[24]H. Baker (Ed.), et. al, **"ASM Handbook, V. 3 Alloy Phase Diagrams,"** ASM Intl., 1992).

[25]P.T. Sarjeant and R. Roy, **"A New Approach to the Prediction of Glass Formation,"** Mat. Res. Bull., 3, 265-280 (1968).
[26] Technical Data Summary for the Defense Waste Processing Facility Sludge Plant, U.S. DOE Report DPSTD 80-38-2, E.I. duPont deNemours &Co., Aiken, SC (September 1982).
[27]J.P. Mosley, **"Calculated Physical Properties of SRP Waste Glasses Using Frit 131,"** U.S. DOE Report DPST-80-724, E.I. duPont deNemours &Co., Aiken, SC (December 1980).
[28]P.D. Soper and D.F. Bickford, **"Physical Properties of Frit 165/Waste Glasses,"** U.S. DOE Report DPST-82-899, E.I. duPont deNemours &Co., Aiken, SC (October 1982).
[29]W.P. Colven, D.M. Sabatino, J.L. Kessler, H.C. Wolf, **"Summary of the Fifth Run of the Large Slurry-Fed Melter,"** U.S. DOE Report DPST-82-890, E.I. duPont deNemours & Co., Savannah River Lab., Aiken, SC (September, 1984).
[30]D.R. Uhlmann and H. Yinnon, **"The Formation of Glasses**" in Glass Science and Technology, V.1, 1-47 (1983).
[31] K.L. Luthra, "**A Comparison of the Mechanism of Oxidation of Ti- and Ni-base Alloys**," Environ. Eff. Adv. Mater., (R.H. Jones and R.E. Ricker, Minerals, Metals and Materials Society, Warrendale, PA, 123-131 (1991).
[32]A.D. Pelton, H. Schmalzried, and J. Sticher, J. Phys. Chem. Solids, 40 [12], 1103-1122 (1979) see also Phase Diagrams for Ceram. Figure 6270, Vol VI, Am. Ceram. Soc., Westerville, OH (1987).
[33]A. Muan and E.F. Osborn, **"Phase Equilibria Among Oxides in Steelmaking,"** Addison-Wesley Publ. Co., Reading MA (1965).